ISSN 1063-7834, Physics of the Solid State, 2021, Vol. 63, No. 6, pp. 897–903. © Pleiades Publishing, Ltd., 2021.
ISSN 1063-7834, Physics of the Solid State, 2021. © Pleiades Publishing, Ltd., 2021.
Russian Text © The Author(s), 2021, published in Fizika Tverdogo Tela, 2021, Vol. 63, No. 6, pp. 721–728.

Electrical Properties of the Polycrystalline $BiFe_{0.95}Co_{0.05}O_3$ Films

O. B. Romanova[a, *], V. V. Kretinin[b], S. S. Aplesnin[a, b], M. N. Sitnikov[b], L. V. Udod[a, b], and K. I. Yanushkevich[c]

[a] *Kirensky Institute of Physics, Krasnoyarsk Scientific Center, Siberian Branch, Russian Academy of Sciences, Krasnoyarsk, 660036 Russia*

[b] *Siberian State University of Science and Technology, Krasnoyarsk, 660014 Russia*

[c] *Scientific and Practical Materials Research Center, National Academy of Sciences of Belarus, Minsk, 220072 Belarus*

**e-mail: rob@iph.krasn.ru*

Received January 29, 2021; revised January 29, 2021; accepted January 29, 2021

Abstract—Semiconductor $BiFe_{0.95}Co_{0.05}O_3$ thin-film compounds have been synthesized by a burst technique. The film surface morphology and the effect of electronic doping via substitution of cobalt ions for trivalent iron on the optical, magnetic, and kinetic properties have been investigated in the temperature range of 77–600 K in magnetic fields of up to 12 kOe. Two electron relaxation channels have been found in the impedance spectrum in the frequency range of 0.1–1000 kHz. The negative magnetoresistance in the anomalous magnetization region and the maximum magnetoimpedance in the vicinity of the surface phase transition have been established. Using the Hall measurements, carrier types dominating in the magnetoresistance and magnetoimpedance effects have been determined. The magnetization anomalies have been explained in the model of superparamagnetic clusters and the magnetoresistance, by the carrier scattering by spin fluctuations.

Keywords: semiconductor films, magnetoresistance, magnetoimpedance, magnetization

DOI: 10.1134/S1063783421060184

1. INTRODUCTION

Multiferroics evoke interest both in view of their application in spintronics, sensing technology, and data recording [1–4] and for establishing fundamentals of the magnetoelectric coupling. Bismuth ferrite with a perovskite structure is one of the most popular compounds that serve as a basis of novel magnetoelectric materials. Bismuth ferrite $BiFeO_3$ (BFO) has high temperatures of the electrical (T_c = 1083 K) [5] and magnetic (T_N = 673 K) ordering [6] and undergoes a series of phase transitions accompanied by magnetoelectric anomalies [7, 8].

The conductivity of BFO determined by magnetic and ferroelectric domain walls is higher than the domain conductivity by several orders of magnitude [9]. An increase in the conductivity of bismuth ferrite in the region of a domain wall is caused by a potential barrier near the interface and a decrease in the band gap by 3%. The conductivity of a domain wall can be switched by an electric field, changing its value by more than an order of magnitude, which makes it possible to create memristor devices [10].

The BFO magnetic structure is a spin cycloid; the magnetic moments of iron ions rotate in the (110) plane along the $[110]_{hex}$ direction. The destruction of the cycloid leads to the occurrence of a weak ferromagnetic moment and enhancement of the magnetoelectric effect [10]. In strong magnetic fields, the spin cycloid is suppressed [11] upon substitution of 3*d* elements, e. g., Fe [12] and Mn [13], and during synthesis of the bismuth ferrite-based thin-film compounds [14, 15]. The magnetization of the BFO films can be controlled by an electric field [17].

The properties of a thin film material can be significantly different from the properties of the same material in the bulk state [18]. For example, bismuth ferrite nanotubes undergo a low-temperature surface phase transition at T = 140.3 K, which is accompanied by a change in the lattice parameter and charge density on the surface [19].

In the previously investigated manganese-substituted bismuth ferrite $BiMn_XFe_{1-X}O_3$ ($0 < X < 0.15$) films, a photoinduced diode effect was found in the near-infrared and violet spectral regions in a wide temperature range [20]. The temperature, wavelength, and illumination power dependences of the diode effect have been established. The observed low-temperatures anomalies in the magnetic and dielectric properties were attributed to the elimination of degeneracy of the 3*d* states of cations due to the spin-orbit interaction and the formation of a Coulomb gap in the spectrum of impurity electron excitations. The calculation and experimental studies reported in [21, 22]

showed that the magnetic and electrical properties of BFO can be significantly improved by Co doping in the B sites and the total magnetic moment of a unit cell was ~0.93μ_B for $BiFe_{0.83}Co_{0.17}O_3$. The strong exchange interaction between Co^{3+} and Fe^{3+} in the $BiFe_{1-X}Co_XO_3$ (BFCO) system can significantly affect the interplay of the electrical and magnetic properties. In addition, almost the same ionic radii of Fe^{3+} (0.64 Å) and Co^{3+} (0.54 Å) make it possible to synthesize a BFCO solid solution with a bismuth iron garnet crystal structure [23]. The magnetodielectric effect (ME) detected on the $BiFe_{0.9}Co_{0.09}Mn_{0.01}O_3$ samples is six times stronger than in the initial BFO compound [24]. The ME was found in cobalt-doped nanostructured BFO above room temperature in the low-frequency range [25]. The investigations of the structural and electrical properties of the BFCO and $Bi_{1-X}Nd_XFeO_3$ (BNFO) thin-film compounds synthesized on the $Pt/Ti/SiO_2/Si(111)$ substrates by chemical deposition from solution showed a significant improvement of the ferroelectric properties upon cobalt doping [26].

The aim of this study is to increase the conductivity in comparison with that of bismuth ferrite and establish the effect of a magnetic field on the kinetic properties of the $BiFe_{0.95}Co_{0.05}O_3$ thin-film bismuth ferrite multiferroic compound via electron doping with cobalt ions without changing the crystal structure.

2. MEASURING TECHNIQUE

The phase composition and crystal structure of the synthesized $BiFe_{0.95}Co_{0.05}O_3$ thin-film compounds were examined at room temperature on a DRON-3 X-ray diffractometer (CuK_α radiation) in the pointwise data collection mode. The cross section of the $BiFe_{0.95}Co_{0.05}O_3$ samples was studied by transmission electron microscopy (TEM) on a Hitachi HT7700 microscope. The structure of the IR spectra of the $BiFe_{0.95}Co_{0.05}O_3$ films recorded on an FSM 2202 IR Fourier spectrometer was investigated and identified. The measurements were performed in an optical cryostat in the temperature range of 77–500 K at frequencies of 450–7000 cm^{-1}. The optical absorption spectrum was recorded on a Cary500Scan spectrophotometer at $T = 300$ K. The magnetic properties were studied by the Faraday method in the temperature range of 77–600 K in magnetic fields of up to 8.6 kOe. The electrical measurements were performed in magnetic fields of up to 12 kOe in the temperature range of 77–400 K and the frequency range of ω = 0.1–1000 kHz. The effect of a magnetic field on the transport characteristics was determined from the magnetic field dependence of the electrical resistivity and from the I–V characteristics measured at constant temperatures in zero magnetic field and in a field of 12 kOe. The electrical resistivity and I–V characteristics were measured on the parallelepiped samples in a dc current by a four-probe method. The Hall voltage was measured in the temperature range of 100–400 K in a magnetic field of 12 kOe. The measurements took into account the contributions of parasitic emf induced by side galvanomagnetic and thermomagnetic effects and the asymmetry of contacts (the zero magnetic field measurements).

3. STRUCTURAL, OPTICAL, AND MAGNETIC PROPERTIES

The bismuth ferrite solid solution films were prepared by sputtering of the pre-synthesized $BiFe_{0.95}Co_{0.05}O_3$ solid solutions onto object glasses using the burst technique. The procedure of the synthesis of these thin-film compounds was described in detail in [27]. The deposition was performed in a UVN-71R-2 vacuum system. The pressure in a reaction chamber during deposition was maintained at 10^{-3} Pa. The temperature of a tantalum evaporator was ~2000°C. The substrates were located at a distance of 10 cm from the evaporator and their temperature was varied within 250–300°C. The precursors were powders with a grain size from 0.1 to 0.3 mm; their X-ray diffraction pattern is shown in Fig. 1. The films had geometric sizes of 14 × 17 mm. The X-ray diffraction pattern of the $BiFe_{0.95}Co_{0.05}O_3$ powder compound contains, along with diffraction reflections of the synthesized compound, the reflections that can be attributed to the primary $BiFeO_3$ phase with a rhombohedral structure.

The analysis of high-resolution microphotographs and electron diffraction patterns (Figs. 2a, 2b) shows that the synthesized $BiFe_{0.95}Co_{0.05}O_3$ films are nanocrystalline. The cross-sectional TEM study of the samples showed that their thickness was d ~ 330 nm.

The presence of crystal lattice defects and crystal phases of different symmetries and the electronic structure can be established by IR spectroscopy.

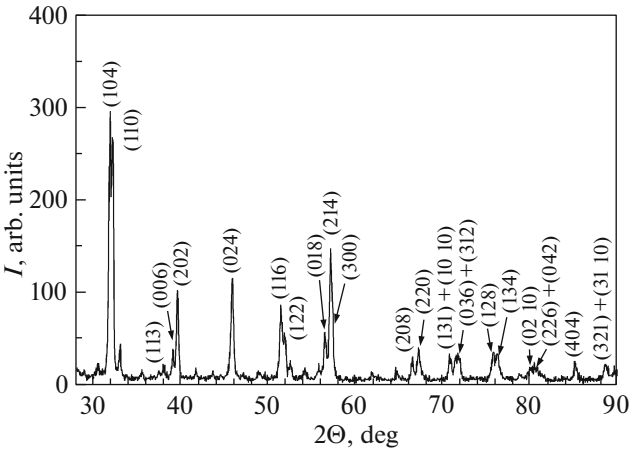

Fig. 1. X-ray diffraction data on the $BiFe_{1-X}Co_XO_3$ system with $X = 0.05$ at 300 K.

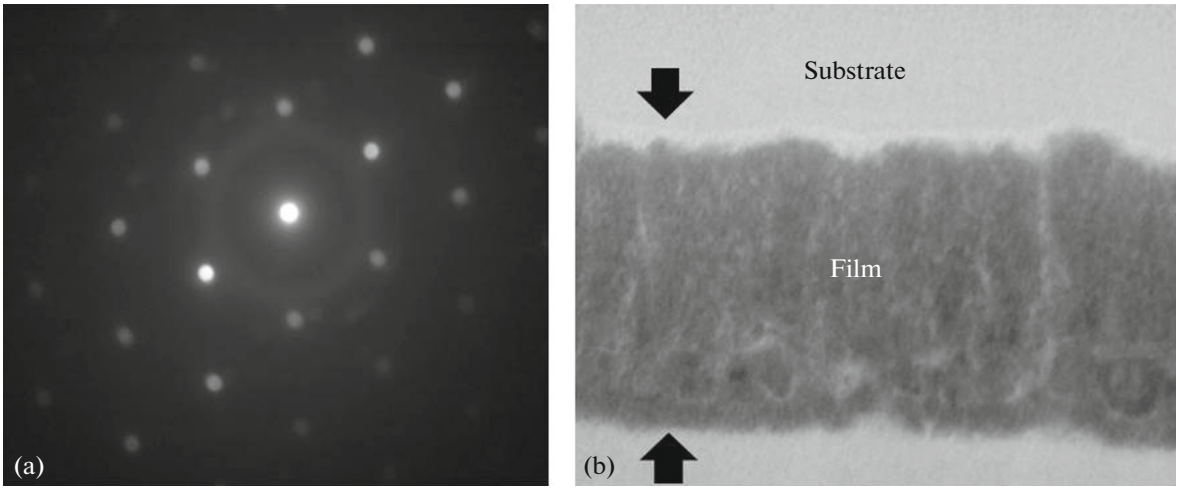

Fig. 2. (a) Electron diffraction pattern and (b) cross-sectional microphotograph of the $BiFe_{0.95}Co_{0.05}O_3$ thin film.

Figure 3 presents IR spectra of the polycrystalline $BiFe_{1-X}Co_XO_3$ films. The cationic substitution of cobalt for iron leads to the appearance of a maximum in the absorption spectra near an energy of 0.072 eV, which vanishes above 320 K. This peak is related to a low-energy electronic transition from the localized states to the edge of the mobility level (Fig. 2a). A decrease in the intensity with increasing temperature can be attributed to the depletion of the impurity level with delocalization of electrons. The band gap E_g of the $BiFe_{0.95}Co_{0.05}O_3$ thin-film compounds was determined from the optical absorption spectra (Fig. 3b). It was found that the E_g value determined by extrapolating the straight portion of the dependence of $(\alpha h\nu)^2$ on the photon energy up to intersection with the abscissa axis is about 2.8 eV. The cationic substitution of cobalt, in contrast to the substitution of manganese, leads to an increase in the gap energy, which is $E_g = 2.4$ eV for $BiFe_{0.95}Mn_{0.05}O_3$ [20].

The magnetic phase transition temperature T_C = 560 K was determined from the temperature dependence of the magnetization of the $BiFe_{0.95}Co_{0.05}O_3$ film measured in a magnetic field of 8.6 kOe (Fig. 4). In the $\sigma(T)$ curve, one can distinguish two temperature ranges of the anomalous magnetization in the vicinity of 140 and 400 K. The magnetization variation in the low-temperature region is caused by the surface phase transition found in the initial BFO [19]. The temperature dependence of the magnetization is qualitatively described in the molecular field approximation $M = M_0(1 - T/T_c)^{1/2}$ (curve *2* in Fig. 4). In the temperature range of 250–500 K, the experimental $\sigma(T)$ data exceed the theoretical values due to the formation of inhomogeneous magnetic states. The anomalous behavior of the magnetization in this temperature range can be described in the model of superparamagnetic clusters with a random distribution of

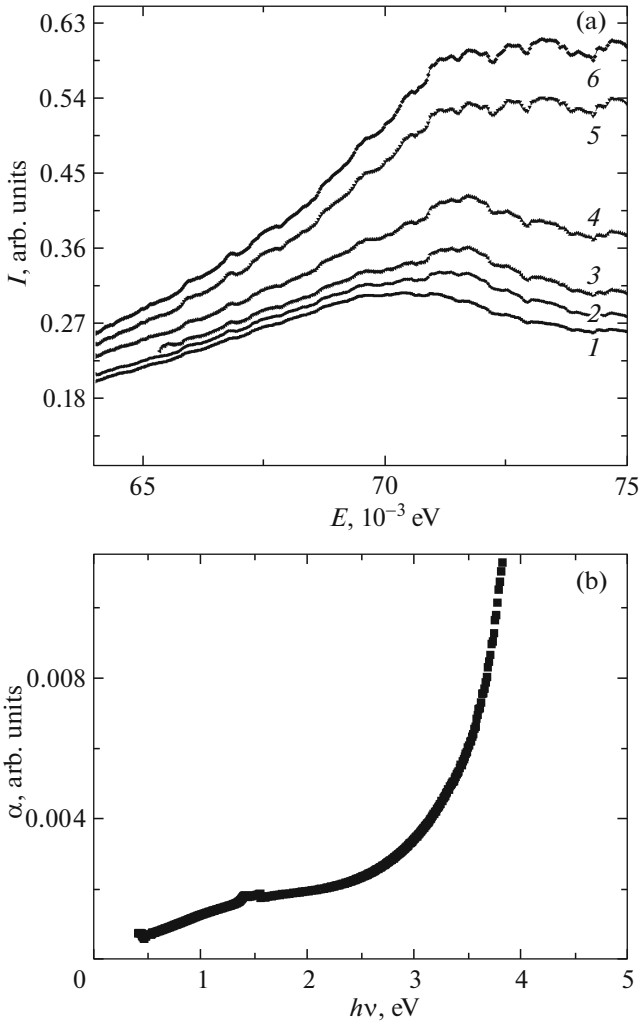

Fig. 3. (a) IR spectra measured at T = (*1*) 80, (*2*) 160, (*3*) 240, (*4*) 320, (*5*) 440, and (*6*) 480 K. (b) Optical absorption spectra of the $BiFe_{0.95}Co_{0.05}O_3$ film measured at T = 300 K.

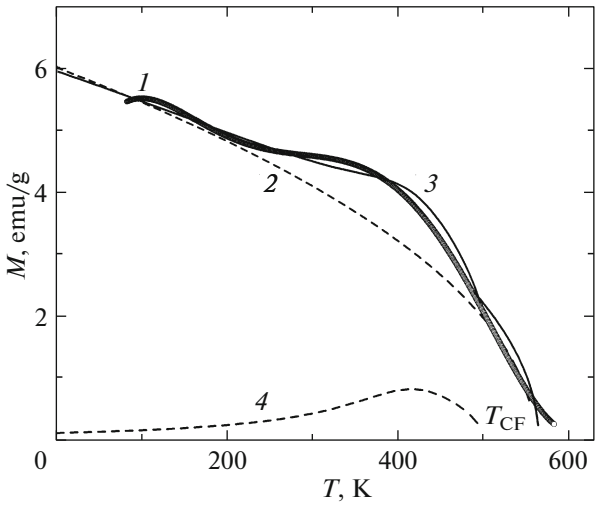

Fig. 4. Temperature dependences of the magnetization for the $BiFe_{0.95}Co_{0.05}O_3$ thin-film compounds in a magnetic field of $H = 8.6$ kOe (curve *1*). Temperature dependence of the magnetization in the molecular field approximation (curve *2*) and the resulting magnetization described by Eq. (2) (curve *3*). Power dependence of the cluster magnetization on temperature (curve *4*).

the anisotropy fields [28]. In the BFO films with the rhombohedral symmetry, the magnetic anisotropy is a power-law function of the magnetization. Below room temperature, the magnetic moments are frozen and, upon heating, tend to align in the external magnetic field direction.

In the model of a superparamagnet with anisotropy field H_A in external magnetic field H, we estimate the contribution of the magnetization formed by inhomogeneous states. We represent the energy of a superparamagnetic cluster in the form $W = M_F H\cos\theta + M_F H_A\cos(\gamma - \theta)$, where the angle θ indicates the magnetic moment direction relative to the applied magnetic field and γ is the angle between the applied magnetic field and anisotropy field directions. The direction of the magnetic moment is determined by $\tan\theta = H_A\sin\gamma/(H + H_A\cos\gamma)$. The longitudinal magnetic susceptibility at $\gamma = \pi/2$ has the form

$$X^Z = M_F\cos(\theta) = M_F/(H\sqrt{(1 + (H_A/H)^2)}). \quad (1)$$

We present the cluster magnetization vs temperature by the power function $M_F = m_{0F}(1 - T/T_{cF})^{1/2}$, where T_{cF} is the critical temperature of a cluster. The anisotropy field vs temperature also has the power-law form $H_A = K(1 - T/T_{cF})^n$. The experimental data are well-described with an exponent of $n = 2$. The resulting magnetization consists of the homogeneous part $M = m_0(1 - T/T_c)^{1/2}$ and the inhomogeneous part

$$M_{res} = m_0\sqrt{(1 - T/T_c)} + m_{0F}\sqrt{(1 - T/T_{cF})}/\sqrt{(1 + (K(1 - T/T_{cF})^2/H)^2)}. \quad (2)$$

The experimental data are satisfactorily described by function (2) with a critical temperature of $T_{cF} = 480$ K (curve *4* in Fig. 4). The replacement of iron by cobalt shifts the magnetic phase transition below the temperature of the magnetic phase transition of $BiFeO_3$.

4. IMPEDANCE, ELECTRICAL RESISTANCE, AND HALL EFFECT

According to the magnetic measurement data, substitution of cobalt for iron forms magnetically inhomogeneous states in the $BiFe_{0.95}Co_{0.05}O_3$ thin-film compound. The existence of these states can also be established by impedance spectroscopy. For the $BiFe_{0.95}Co_{0.05}O_3$ bismuth ferrite films, the real (active resistance R) and imaginary (reactance X) parts of the impedance were measured and the complex impedance Z was determined. It was found that, with an increase in temperature, the R and Z values decrease and their frequency dependences (Figs. 5a, 5b) change. The frequency dependence of the imaginary part X of the impedance is linear.

Using the formula $\delta(Z) = \dfrac{Z(H) - Z(0)}{Z(0)} \times 100\%$, the relative impedance variation in a magnetic field was determined (inset in Fig. 5b). Its maximum value (1.5%) was found in the region of the surface phase transition in the low-frequency range. With an increase in temperature and frequency, the magnetoimpedance changes its sign to positive and tends to zero at high frequencies. The frequency dependence of the impedance is described by a function with two relaxation times in the frequency ranges of $\omega > 5 \times 10^5$ Hz and $\omega < 5 \times 10^5$ Hz (Fig. 5b)

$$Z(\omega) = \frac{A_1}{1 + (\omega\tau_1)^2} + \frac{A_2}{1 + (\omega\tau_2)^2}, \quad (3)$$

where parameters $A_{1,2}$ remain constant and temperature-independent and $\tau_{1,2}$ are the relaxation times. The inset in Fig. 5a shows the relaxation times, which decrease with increasing temperature and take the minimum values in the region of formation of inhomogeneous magnetic states. The relaxation of conduction electrons is related to the energy transfer to the spin subsystem.

The magnetically inhomogeneous state is found in the temperature dependence of the resistivity ρ measured at a dc current. In the temperature range of 260–400 K, a decrease in the ρ is observed (Fig. 6a), which is caused by delocalization of carriers from the impurity states determined from the IR spectra. An increase in the resistance at $T = 400$ K is related to the carrier scattering by spin fluctuations in the vicinity of the magnetic phase transition, which is confirmed by the linear dependence of the resistivity on the squared magnetization (inset in Fig. 6a). The experimental

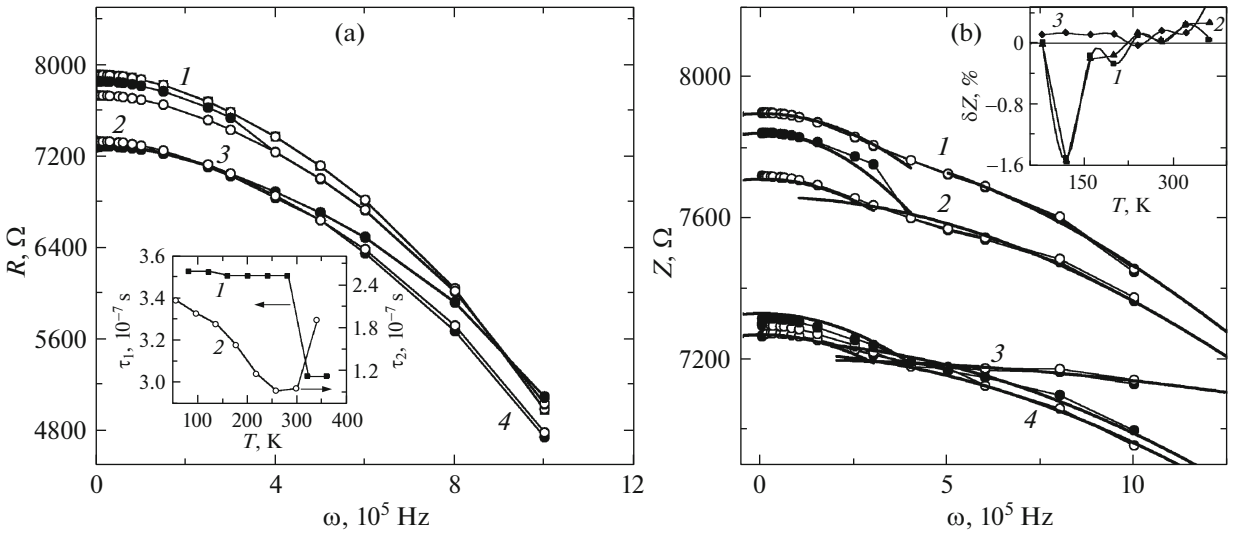

Fig. 5. Frequency dependences of (a) the active resistance and (b) impedance of the $BiFe_{0.95}Co_{0.05}O_3$ films measured in zero magnetic field and in a field of 12 kOe at $T =$ (*1*) 80, (*2*) 120, (*3*) 280, and (*4*) 360 K. Fitting functions, Eq. (3) (solid line). Inset in (a): temperature dependence of relaxation times $\tau_1(1)$ and $\tau_2(2)$. Inset in (b): temperature dependence of the relative impedance variation $\delta(Z) = \dfrac{Z(H = 12\text{ kOe}) - Z(H = 0)}{Z(H = 0)} \times 100\%$ measured at frequencies of (*1*) 10^2, (*2*) 10^4, and (*3*) 10^6 Hz.

data on the resistivity are in good agreement with the theoretical calculation in the dynamic molecular field (DMF) approximation [29, 30]. In this model, the resistivity depends on the magnetization according to the law [31]

$$\frac{\rho(M)}{\rho(M = 400\text{ K})} = 1 - CM^2, \qquad (4)$$

where C is the temperature- and magnetic-field- independent numerical constant. Thus, the functional $\rho(T, H)$ dependence arises through the magnetization $M = M(T, H)$. This means that the electrical resistivity is fully determined by the carrier scattering by fluctuations of the magnetic order. In the weak-coupling limit, we have $J_H \ll W$ (in the Born approximation), $C = 1$ [32]; however, in the case of a strong coupling $J_H \gg W$ and, as follows from the DMF calculation, $C > 1$ [33]. In the $BiFe_{1-X}Co_XO_3$ system with a substitution concentration of $X = 0.05$, we have $C = 0.4$ and the weak coupling is implemented.

The behavior of the temperature dependence of the impedance measured on an ac current is qualitatively different from the behavior of the resistivity measured on a dc current (Fig. 6b). As the temperature rises, the Z values decrease and depend on frequency. There are two $Z(T)$ anomalies. In the temperature range of 156–175 K, the impedance grows and the temperature of the minimum is frequency-independent, which is typical of structural phase transitions. The other anomaly in the form of a step is 0.5% and manifests itself at $T = 360$ K.

The effect of the magnetic field on the transport properties was determined from the I–V characteristics measured in zero magnetic field and in a field of 12 kOe at temperatures of 300, 340, and 380 K (Fig. 7a). The I–V characteristics are linear and weakly depend on the applied magnetic field. This is evidenced by the magnetoresistance determined by the formula $\delta_H = \dfrac{R(H) - R(0)}{R(0)}$, where $R(H)$ is the electrical resistivity in a magnetic field and $R(0)$ is the resistivity without field (inset in Fig. 7a). The negative magnetoresistance exists in the region of magnetically inhomogeneous states and its value increases with temperature, attaining a value of -0.04% at $T =$ 380 K. The $R(H)$ dependences confirm a decrease in the resistivity in a magnetic field. The normalized resistance $(1 - R(H))/R(0))$ is shown in Fig. 7b.

To explain the experimental results, a model of superparamagnetic clusters with a random orientation of the anisotropy axis and orbital angular momenta was used. A significant contribution to the resistivity variation with the applied field will give rise to hoppings over clusters. The proposed model includes hopping over a lattice with the matrix elements depending on the mutual orientation of spins on the sites. The hopping probability increases when the magnetic moments are parallel and decreases at the other magnetization directions. The field dependence of the normalized resistance is described by the function [34]

$$(R(H) - R(0))/R(0) = \exp(-BH\xi/k_BT) - 1, \qquad (5)$$

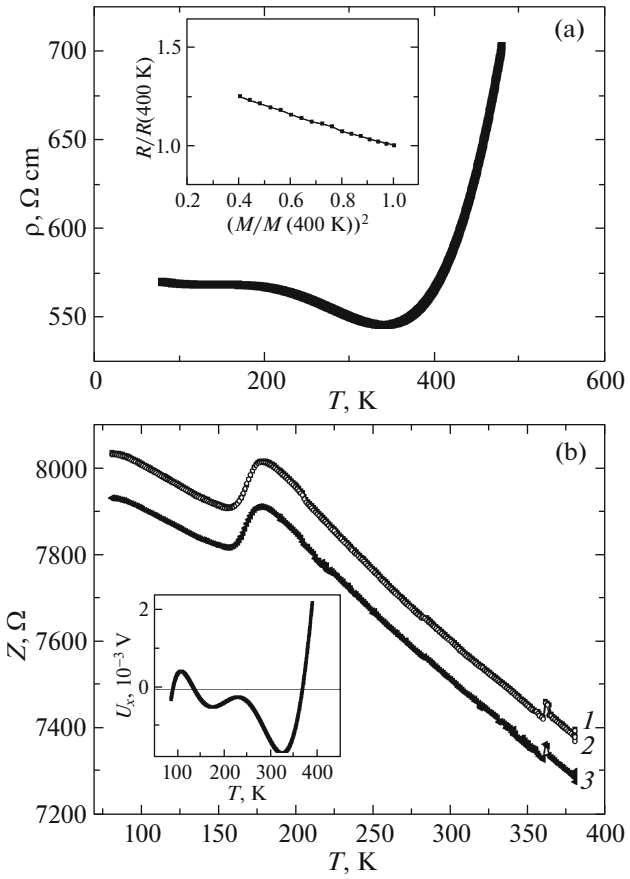

Fig. 6. Temperature dependence of (a) the electrical resistivity measured at $H = 0$ kOe and (b) impedance at frequencies of ω = (*1*) 1, (*2*) 50, and (*3*) 300 kHz for the $BiFe_{0.95}Co_{0.05}O_3$ film samples. Inset in (a): magnetization dependence of the resistivity. Inset in (b): temperature dependence of the Hall voltage for the same sample.

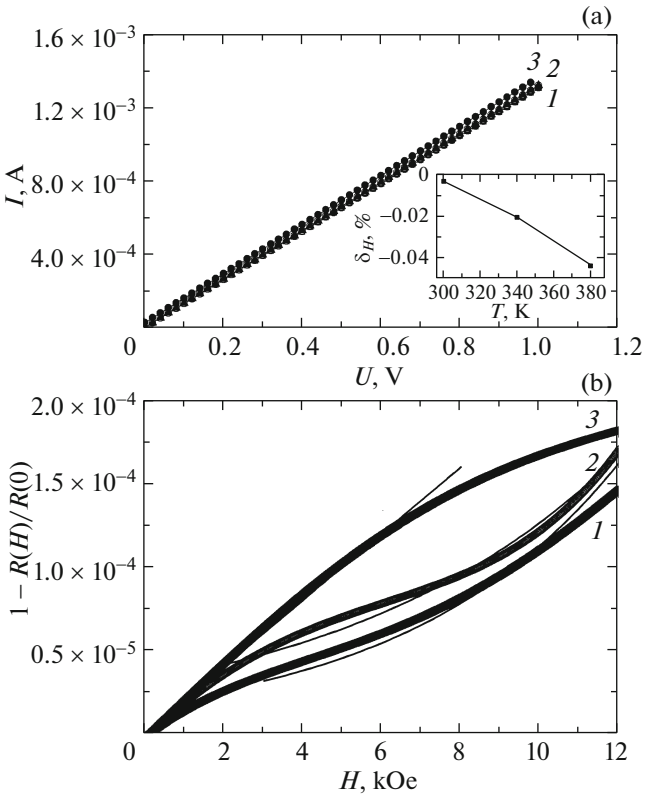

Fig. 7. (a) *I–V* characteristics measured in zero magnetic field and in a field of 12 kOe for the $BiFe_{0.95}Co_{0.05}O_3$ films at T = (*1*) 300, (*2*) 340, and (*3*) 380 K. (b) Field dependences of the normalized resistance measured at T = (*1*) 300, (*2*) 320, and (*3*) 360 K. Inset in (a): temperature dependence of the magnetoresistance $\delta_H = \frac{R(H = 12\text{ kOe}) - R(H = 0)}{R(H = 0)} \times 100\%$. Fitting function described by Eq. (5) (solid line).

where B is determined by the combination of the energies of the Coulomb interaction of electrons in the impurity region, H is the external magnetic field, and ξ is the electron localization radius.

The dominant contribution of electrons or holes to the magnetotransport properties is determined by measuring the Hall voltage in a magnetic field of 12 kOe.

The inset in Fig. 6b shows the temperature dependence of Hall voltage U_X for $BiFe_{0.95}Co_{0.05}O_3$. As the temperature rises, two temperature ranges with a change in the Hall voltage sign are distinguished. The first region (100 K < T < 140 K) correlates with these structural properties and corresponds to a low-temperature surface phase transition. Upon heating, the Hall voltage passes through a minimum at 320 K and changes its sign from negative to positive at T = 360 K, which points out a change in the carrier type from electrons to holes. Possibly, the change in the carrier sign leads to the local compensation of ionized impurities and to the impedance jump (Fig. 6b).

5. CONCLUSIONS

Electron doping of iron with cobalt of the BFO multiferroic in the $BiFe_{1-X}Co_XO_3$ thin-film compounds with a substitution concentration of $X = 0.05$ leads to an increase in the conductivity by several orders of magnitude. We established a decrease in the electrical resistivity upon variation in both the magnetic field and temperature in the region of existence of the inhomogeneous magnetic states determined from the temperature dependences of the magnetization described in the molecular field approximation. The resistivity growth in the vicinity of the magnetic phase transition is caused by the carrier scattering by spin fluctuations. In the absorption spectra, a maximum was observed near an energy of 0.072 eV, which was attributed to the low-energy electronic transition from the localized states to the mobility level edge. The negative magnetoresistance was related to an increase in the probability of the transition of electrons

between clusters with parallel orientation of magnetic moments in a magnetic field.

The maximum change in the magnetoimpedance was found in the low-frequency region in the vicinity of the low-temperature surface phase transition. The times of relaxation of conduction electrons related to the energy transfer to the spin subsystem were determined. A change in the carrier sign in the region of the magnetoimpedance and magnetoresistance maxima was established. The correlation between the magnetic and kinetic properties of the $BiFe_{0.95}Co_{0.05}O_3$ films upon temperature variation was found.

ACKNOWLEDGMENTS

The authors are grateful to the Krasnoyarsk Regional Center for Collective Use of the Krasnoyarsk Scientific Center, Siberian Branch of the Russian Academy of Sciences for offering the opportunity to study the surface morphology of the $BiFe_{0.95}Co_{0.05}O_3$ films.

FUNDING

This study was supported by the Russian Foundation for Basic Research and the Belarusian Republican Foundation for Basic Research, project no. 20-52-00005.

CONFLICT OF INTEREST

The authors declare that they have no conflicts of interest.

REFERENCES

1. H. Béa, M. Gajek, M. Bibes, and A. Barthélémy, J. Phys.: Condens. Matter **20**, 434221 (2008).
2. S. Saremi, R. Xu, L. R. Dedon, R. Gao, A. Ghosh, A. Dasgupta, and L. W. Martin, Adv. Mater. Interfaces **5**, 1700991 (2018).
3. W. Eerenstein, N. D. Mathur, and J. F. Scott, Nature (London, U.K.) **442**, 759 (2006).
4. Xi Chen, A. Hochstrat, P. Borisov, and W. Kleemann, Appl. Phys. Lett. **89**, 202508 (2006).
5. J. R. Teague, R. Gerson, and W. J. James, Solid State Commun. **8**, 1073 (1970).
6. P. Fischer, M. Polomska, I. Sosnowska, and M. Szymanski, J. Phys. C **13**, 1931 (1980).
7. R. Palai, R. S. Katiyar, H. Schmid, P. Tissot, S. J. Clark, J. Robertson, S. A. T. Redfern, G. Catalan, and J. F. Scott, Phys. Rev. B **77**, 014110 (2008).
8. N. Ortega, A. Kumar, P. Bhattacharya, and S. B. Majumder, Phys. Rev. B **77**, 014111 (2008).
9. S. Farokhipoor and B. Noheda, Phys. Rev. Lett. **107**, 127601 (2011).
10. P. Maksymovych, J. Seidel, Y. H. Chu, P. Wu, A. P. Baddorf, L. Q. Chen, S. I. Kalinin, and R. Ramesh, Nano Lett. **11**, 1906 (2011).
11. G. Catalan and J. F. Scott, Adv. Mater. **21**, 2463 (2009).
12. Yu. F. Popov, A. M. Kadomtseva, G. P. Vorob'ev, and A. K. Zvezdin, Ferroelectics **162**, 135 (1994).
13. Feng Yan, Guozhong Xing, Rongming Wang, and Lin Li, Sci. Rep. **5**, 9128 (2015).
14. I. Sosnowska, W. Schäfer, W. Kockelmann, K. H. Andersen, and I. O. Troyanchuk, Appl. Phys. A **74**, s1040 (2002).
15. J. Wang, J. B. Neaton, H. Zheng, V. Nagarajan, S. B. Ogale, B. Liu, D. Viehland, V. Vaithyanathan, D. G. Schlom, U. V. Waghmare, N. A. Spaldin, K. M. Rabe, M. Wutting, and R. Ramesh, Science (Washington, DC, U. S.) **299** (5613), 1719 (2003).
16. J. Li, J. Wang, M. Wutting, R. Ramesh, N. Wang, B. Ruette, A. P. Pyatakov, A. K. Zvezdin, and D. Viehland, Appl. Phys. Lett. **84**, 5261 (2004).
17. T. Zhao, A. Scholl, F. Zavaliche, K. Lee, M. Barry, A. Doran, M. P. Cruz, Y. H. Chu, C. Ederer, N. A. Spaldin, R. R. Das, D. M. Kim, S. H. Baek, C. B. Eom, and R. Ramesh, Nat. Mater. **5**, 823 (2006).
18. A. Ohtomo and H. Y. Hwang, Nature (London, U.K.) **427**, 423 (2004).
19. R. Jarrier, X. Marti, J. Herrero-Albillos, P. Ferrer, R. Haumont, P. Gemeiner, G. Geneste, P. Berthet, T. Schülli, P. Cevc, R. Blinc, S. S. Wong, Tae-Jin Park, M. Alexe, M. A. Carpenter, J. F. Scott, G. Catalan, and B. Dkhil, Phys. Rev. B **85**, 184104 (2012).
20. S. S. Aplesnin, V. V. Kretinin, A. N. Masyugin, O. B. Romanova, M. N. Sitnikov, O. B. Begisheva, A. I. Galyas, O. F. Demidenko, and K. I. Yanushkevich, Semicond. Sci. Technol. **34**, 095007 (2019).
21. Y. Sui, Ch. Xin, X. Zhang, Y. Wang, Y. Wang, X. Wang, Zh. Liu, B. Li, and X. Liu, J. Alloys Compd. **645** (5), 78 (2015).
22. K. Chakrabarti, B. Sarkr, V. D. Ashok, S. S. Chaudhari, and S. K. De, J. Magn. Magn. Mater. **381**, 271 (2015).
23. V. A. Reddy, N. P. Pathak, and R. Nath, Solid State Commun. **171**, 40 (2013).
24. A. Marzouki, V. Loyau, P. Gemeiner, L. Bessais, B. Dkhil, and A. Megriche, J. Magn. Magn. Mater. **498**, 166137 (2020).
25. V. G. Shrimali, K. Gadani, K. N. Rathod, B. Rajyaguru, A. D. Joshi, D. D. Pandya, P. S. Solanki, and N. A. Shan, Mater. Chem. Phys. **228**, 98 (2019).
26. Y.-L. Zhang, N. Yan, X.-J. Wang, S. Chen, and Sh.-H. Yang, Ferroelectrics **454**, 35 (2013).
27. O. B. Romanova, S. S. Aplesnin, M. N. Sitnikov, L. V. Udod, O. B. Begisheva, and O. F. Demidenko, J. Mater Sci. Mater. Electron. **918**, 012101 (2020).
28. S. Yunoki, J. Hu, A. L. Malvezzi, A. Moreo, N. Furukawa, and E. Dagotto, Phys. Rev. Lett. **80**, 845 (1998).
29. N. Furukawa, J. Phys. Soc. Jpn. **63**, 3214 (1994).
30. N. Furukawa, J. Phys. Soc. Jpn. **64**, 2734 (1995).
31. Yu. A. Izyumov and Yu. N. Skryabin, Phys. Usp. **44**, 109 (2001).
32. T. Kasuya, Prog. Theor. Exp. Phys. **16**, 58 (1956).
33. Y. Tokura, A. Urushibara, Y. Moritomo, T. Arima, A. Asamitsu, G. Kido, and N. Furukawa, J. Phys. Soc. Jpn. **63**, 3931 (1994).
34. M. Yu. Kagan and K. I. Kugel', Phys. Usp. **44**, 553 (2001).

Translated by E. Bondareva